method reported previously [20]. In a typical procedure to synthesize the MWCNT/CdS core–shell nanowires, 14 mg purified MWCNTs were added into dry tetrahydrofuran (THF), which contained 0.1–0.4 mmol S (99.999 %) powder and an identical stoichiometric amount of anhydrous $CdCl_2$. After ultrasonical dispersion for 30 min, excess KBH_4 was slowly added to the flask under vigorous stirring at room temperature. The S was reduced to S^{2-} and the suspension gradually turned light yellow. After the mixture was stirred for 12 h, a dark yellow precipitate was produced. The dark yellow powder was filtered and washed thoroughly with dry THF, deionized water, and absolute ethanol several times to remove the impurities.

The products were characterized by TEM (JEM-200CX), powder XRD (Rigaku D/max diffractometer), and EDX. SPS was measured with a standard metal–insulator–semiconductor (MIS) approach using a steady-state chopped light source monochromator-lock-in detection technique. The tablet samples were sandwiched between two indium tin oxide (ITO) electrodes, with air as the insulating layer (ITO/insulator (air)/sample/ITO). Monochromatic light was obtained by passing light from a 500 W xenon lamp through a grating monochromator. A lock-in amplifier (Stanford SR 830), synchronized with a light chopper (Stanford SR 540), was employed to amplify the photovoltage signal. The principle and the illustration of the SPS were discussed in detail in [18].

Received: September 1, 2003
Final version: October 10, 2003

[1] S. Iijima, *Nature* **1991**, *354*, 56.
[2] T. Rueckes, K. Kim, E. Joselevich, C. M. Lieber, *Science* **2000**, *289*, 94.
[3] S. Saito, *Science* **1997**, *278*, 77.
[4] R. J. Chen, Y. Zhang, D. Wang, H. J. Dai, *J. Am. Chem. Soc.* **2001**, *123*, 3838.
[5] X. Y. Gong, J. Liu, S. Baskaran, R. D. Voise, J. S. Yang, *Chem. Mater.* **2000**, *12*, 1049.
[6] B. Azamian, J. Davis, K. Coleman, C. Bagshaw, M. L. H. Green, *J. Am. Chem. Soc.* **2002**, *124*, 12 664.
[7] T. Seeger, T. Köhler, T. Frauenheim, N. Grobert, M. Rühle, M. Terrones, G. Seifert, *Chem. Commun.* **2001**, 34.
[8] J. Kong, M. Chapline, H. Dai, *Adv. Mater.* **2001**, *13*, 1384.
[9] K. Hernadi, E. Ljubovic, J. W. Seo, L. Forró, *Acta Mater.* **2003**, *51*, 1447.
[10] S. W. Lee, W. M. Sigmund, *Chem. Commun.* **2003**, 780.
[11] S. Banerjee, S. S. Wong, *Nano Lett.* **2002**, *2*, 195.
[12] S. Banerjee, S. S. Wong, *J. Am. Chem. Soc.* **2003**, *125*, 10 342.
[13] J. M. Haremza, M. A. Hahn, T. D. Krauss, *Nano Lett.* **2002**, *2*, 1253.
[14] S. Ravindran, S. Chaudhary, B. Colburn, M. Ozkan, C. S. Ozkan, *Nano Lett.* **2003**, *3*, 447.
[15] M. S. Strano, C. A. Dyke, M. L. Usrey, P. W. Barone, M. J. Allen, H. Shan, C. Kittrell, R. H. Hauge, J. M. Tour, R. E. Smalley, *Science* **2003**, *301*, 1519.
[16] J. H. Zeng, J. Yang, Y. Zhu, Y. F. Liu, Y. T. Qian, H. G. Zheng, *Chem. Commun.* **2001**, 1332.
[17] H. Cao, Y. Xu, J. Hong, H. Liu, G. Yin, B. Li, C. Tie, Z. Xu, *Adv. Mater.* **2001**, *13*, 1393.
[18] L. Kronik, Y. Shapira, *Surf. Sci. Rep.* **1999**, *37*, 1.
[19] X. Zhao, M. Ohkohchi, M. Wang, S. Iijima, T. Ichihashi, Y. Ando, *Carbon* **1997**, *35*, 775.
[20] I. W. Chiang, B. E. Brinson, R. E. Smalley, J. L. Margrave, R. H. Hauge, *J. Phys. Chem. B* **2001**, *105*, 1157.
[21] L. Cao, H. Z. Chen, H. B. Zhou, L. Zhu, J. Z. Sun, X. B. Zhang, J. M. Xu, M. Wang, *Adv. Mater.* **2003**, *15*, 909.
[22] I. Krau, D. K. Pandya, K. L. Chopra, *J. Electrochem. Soc.* **1980**, *127*, 943.
[23] J. Cao, J. Z. Sun, M. Wang, H. Z. Chen, X. Q. Zhou, D. J. Wang, *Thin Solid Films* **2003**, *429*, 152.
[24] D. B. Romero, M. Carrard, L. Zuppiroli, *Adv. Mater.* **1996**, *8*, 899.
[25] H. Ago, M. S. P. Shaffer, D. S. Ginger, *Phys. Rev. B* **2000**, *61*, 2286.

Electroluminescence in n-ZnO Nanorod Arrays Vertically Grown on p-GaN**

By *Won Il Park* and *Gyu-Chul Yi**

ZnO is a promising material for short-wavelength photonic device applications due to its characteristic direct and wide bandgap with a large exciton binding energy of 60 meV.[1] Recently, both ZnO epitaxial films and single crystalline nanorods have shown excellent optical characteristics.[2–5] Further research on ZnMgO alloys has enabled the control of the bandgap energy in ZnO-based materials and the fabrication of ZnO/ZnMgO nanorod quantum structures.[6] Despite significant progress on ZnO films and nanostructures, the difficulty of p-type doping in ZnO has impeded the fabrication of ZnO p–n homojunction devices. As an alternative approach to homojunction, an n-ZnO/p-GaN heterojunction has been suggested as a strong candidate for device applications,[7,8] since these materials have a similar fundamental bandgap energy (~3.4 eV), the same wurtzite crystal structure, and a low lattice constant misfit of 1.9 %. In general, however, p–n heterojunction devices show a lower efficiency than homojunction devices,[9] because an energy barrier formed at the junction interface decreases carrier injection efficiency for heterojunction devices with a large band offset.[10] This problem may be solved by increasing the carrier injection efficiency by making nanosized junctions, since, as previously reported, the carrier injection rate significantly increases for nanocontacts in Schottky diodes.[11,12] Here, we report on the fabrication of n-ZnO/p-GaN nanorod electroluminescent (EL) devices and their EL characteristics.

A schematic of n-ZnO/p-GaN nanorod heterojunction arrays is shown in Figure 1a. For EL device fabrication, vertically well-aligned n-type ZnO nanorod arrays were epitaxially grown on p-GaN(0001) substrates employing catalyst-free metal-organic vapor phase epitaxy (MOVPE). The growth parameters of ZnO nanorods on GaN(0001) substrates were similar to those on Al_2O_3(0001) substrates.[13] The synthesis of ZnO nanorods resulted in a preferential growth direction along the *c*-axis of ZnO normal to the substrate surface. As shown in Figure 1b, field-emission scanning electron micros-

[*] Prof. G.-C. Yi, W. I. Park
Department of Materials Science and Engineering
Pohang University of Science and Technology (POSTECH)
Pohang, Kyungbuk 790–784 (Korea)
E-mail: gcyi@postech.ac.kr

[**] This research was performed with the financial support of the Center for Nanostructured Materials Technology under the 21st Century Frontier R&D Program of the Ministry of Science and Technology, Korea.

DOI: 10.1002/adma.200305729

ADVANCED MATERIALS

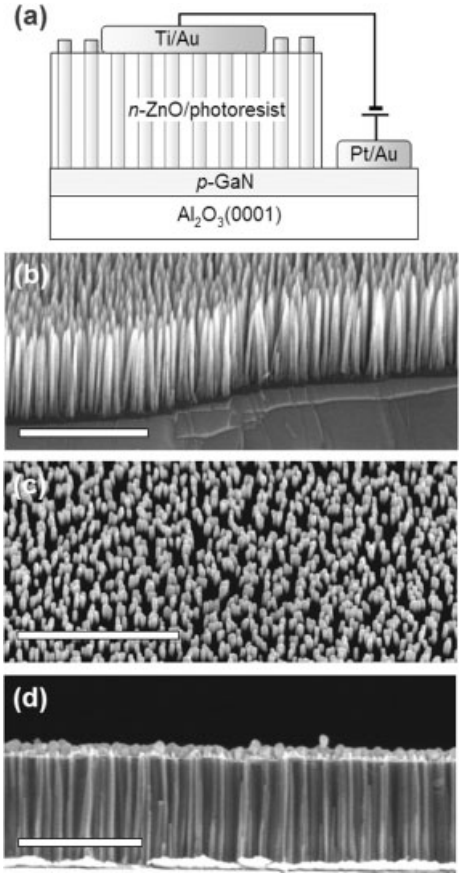

Figure 1. a) Schematic illustration of a p-GaN/n-ZnO nanorod heterostructure device. b) FESEM images of ZnO nanorod arrays grown on p-GaN. ZnO nanorods are well-aligned perpendicular to the GaN surface. c) SEM images of the nanorod tips exposed by selective etching of the photoresist under an oxygen plasma. d) Cross-sectional SEM images of the nanorod heterostructure device fabricated by depositing a Au/Ti metal bilayer on the selectively etched nanorod tips. All scale bars are 1 μm.

copy (FESEM) clearly revealed the general morphology of the ZnO nanorod arrays on p-GaN, showing uniform distributions in their diameters and lengths. The average length and diameter of the nanorods grown for 1 h are 1 μm and 40 nm, respectively. The number density of nanorods was as high as 10^8 per mm^2.

Ohmic contacts were fabricated simply by evaporating Pt/Au and Ti/Au bilayers on p-GaN and n-ZnO, respectively. After metallization of p-GaN, the gaps between the nanorods were filled with a thin photoresist. Selective etching of the photoresist under an oxygen plasma then exposed the nanorod tips, by 50–100 nm, as shown in Figue 1c. Ti and Au were evaporated on the nanorod tips through a shadow mask, resulting in a continuous contact layer on the ZnO nanorod arrays (Fig. 1d). Good ohmic contacts on both n-ZnO and p-GaN were made by rapid thermal annealing.

EL spectra of the n-ZnO/p-GaN nanorod EL devices were measured at various reverse-bias voltages, since no light emission was observed in the measured visible spectrum range for forward-bias voltages up to 10 V. As shown in Figure 2, the

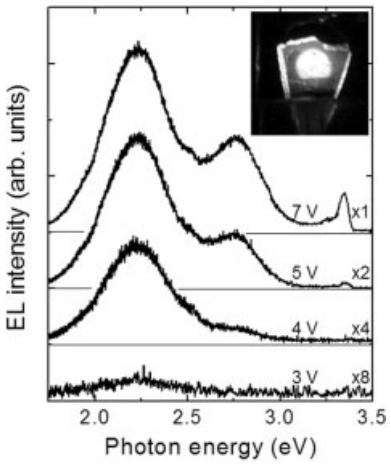

Figure 2. Room temperature EL spectra of a p-GaN/n-ZnO heterojunction device. For reverse-bias voltages larger than 3 V, the EL spectra exhibited a yellow emission band centered at 560 nm (2.2 eV). A weak blue emission band centered at 450 nm (2.8 eV) appeared for reverse-bias voltages larger than 4 V. By further increasing the reverse-bias voltage to 5 V, the blue emission peak intensity increased and an additional ultraviolet emission peak was observed at 3.35 eV. The inset is a photograph of light emission from the EL device at a bias voltage of 5 V. The electroluminescence was strong enough to be observed clearly by the naked eye.

nanorod EL device showed different EL spectra, depending on the reverse-bias voltage. The EL spectrum at an applied reverse-bias voltage of 3 V showed a broad yellow emission band centered at 560 nm (2.2 eV). As the applied reverse-bias voltage increased from 3 to 7 V, the EL emission at 2.2 eV showed a drastic increase in its intensity without exhibiting any peak shift. For reverse-bias voltages above 4 V, however, the EL spectra exhibited an additional weak blue emission at 2.8 eV. By further increasing the reverse-bias voltage to 5 V, the blue emission peak increased and an ultraviolet (UV) emission peak was observed at 3.35 eV.

The EL peaks result from band edge and defect states in ZnO or GaN. The origins of the EL emission peaks were investigated by comparing the EL and photoluminescence (PL) spectra of n-ZnO/p-GaN nanorod heterostructures measured under front- and back-side light excitations (see the insets in Fig. 3). As shown in Figures 3b,c, the PL spectra were strongly dependent on the excitation measurement geometry. That is, for front-side illumination, a dominant PL peak was observed at 3.29 eV, corresponding to the band-edge emission of ZnO. When magnified twenty times, a very weak and broad yellow emission peak at 2.2 eV could be observed: attributable to a defect-related radiative transition in ZnO.[14] The PL spectrum measured under back-side illumination exhibited a dominant blue emission band centered at 2.9 eV and a weak UV peak at 3.45 eV. A blue emission band is generally observed in Mg doped p-GaN epilayers and is attributed to a radiative recombination related to Mg acceptors.[15] The PL data strongly suggest that the yellow and blue emissions in the EL spectra originate from the deep level in the ZnO and the Mg acceptor level in GaN, respectively.

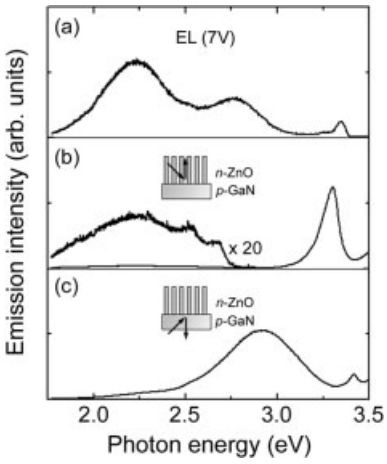

Figure 3. a) EL spectrum and b) front- and c) back-side illuminated PL spectra of a n-ZnO/p-GaN heterojunction nanorod array.

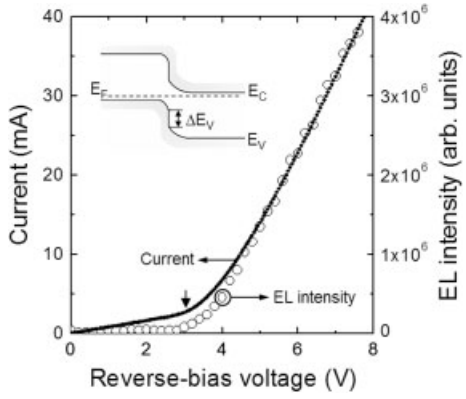

Figure 4. *I–V* characteristics and current–EL intensity measured at a 560 nm yellow emission band of a n-ZnO/p-GaN heterojunction device. For reverse-bias voltages above 3 V, both the light emission intensity and the current increased drastically with the reverse-bias voltage. The inset shows the expected energy-band diagram of a p-GaN/n-ZnO heterojunction device.

The assignment of the EL peak origins explains the EL spectra dependence on the reverse-bias voltage. For low reverse-bias voltages, below 3 V, yellow EL was dominant from the ZnO at the interface between ZnO and GaN, presumably due to the high concentration of defects formed in ZnO at the heterojunction interface. High-resolution transmission electron microscopy confirmed that more defects are formed at the interface than inside the nanorods, although the ZnO layer at the interface was heteroepitaxially grown on the GaN layer without any observable formation of another phase (e.g., gallium oxide) or amorphous layers.[16] As the bias voltage increased, the depletion layer width in p-GaN increased and EL peaks from p-GaN also appeared. In addition to the yellow emission from ZnO, a blue EL peak from the Mg acceptors in the GaN and GaN band edge ultraviolet emission at 3.35 eV were observed for the reverse-bias voltages above 4 and 5 V, respectively. Furthermore, the ratio of the blue emission to the band edge emission decreased with increasing reverse-bias voltage, which implies that the p-type carrier concentration decreased with increasing depth from the heterojunction interface. This may result from the difficulty in dissociating Mg–H complexes to the Mg acceptors deep inside GaN during post-thermal treatment.[17]

Light emission only under reverse-bias indicates that the EL mechanism is different from that of conventional forward-biased p–n junction light emitting diodes. Figure 4 shows the emission intensity and current as a function of reverse-bias voltage. At a reverse-bias voltage of 3 V, both the current and light emission intensity began to increase rapidly with the bias voltage, presumably as a result of electron transport involving tunneling through the heterojunction.[18] Furthermore, the turn-on voltage in the *I–V* plot was almost same as that in the EL plot, strongly suggesting that the EL emission process involves carrier transport through this junction.

Carrier transport at the reverse-bias is explained in terms of band alignment of the p-GaN/n-ZnO heterojunction at the interface. As shown in the inset of Figure 4, a ZnO/GaN heterojunction exhibits type II band alignment, where a calculated valence band offset (ΔE_v) varies from 1.0 to 2.2 eV, with an average value of 1.6 eV, depending on the interface configuration.[19] Since a large band offset formed at the heterojunction lowers the n-ZnO conduction band or raises the p-GaN valence band, the thickness of the tunneling barrier is very thin. With a small reverse-bias voltage, the unoccupied conduction band minimum of n-ZnO would be lower than the occupied valance band maximum of p-GaN. Hence carrier transport by tunneling can occur even at small reverse-bias voltages and the tunneling probability increases with reverse-bias voltage.

Light emission was strong enough to be observed clearly with the naked eye, which may be a characteristic of a nanojunction. In large-area junctions of bulk devices, the depletion width is generally proportional to the Debye length (L_D). Here, interface and edge effects are negligible. As the junction area decreases, however, these effects become dominant and significantly affect the device characteristics.[18] Furthermore, a high electric field might be induced on the p-GaN beneath ZnO nanorods with high aspect ratios. Accordingly, these effects reduce the depletion width of p-GaN, thus increasing the tunneling probability. Hence, it is suggested that electroluminescence of nanojunction EL devices is enhanced due to the increased contribution of tunneling to the total current.

Our vertically aligned ZnO nanorod heteroepitaxial growth by catalyst-free MOVPE creates significant opportunities for the fabrication of photonic and electronic nanodevice arrays. Simple heteroepitaxial growth yields vertically aligned ZnO nanorods with a clean interface on GaN, resulting in the formation of nanosized junctions. The p–n heterojunction nanorod EL devices showed a high current density and strong electroluminescence, even at a reverse-bias voltage of 3 V. More generally, we believe that the simple "bottom up" heteroepitaxial approach might readily be expanded to fabricate many other heteroepitaxial semiconductor nanorod EL devices and arrays.

ADVANCED MATERIALS

Experimental

For the fabrication of n-ZnO/p-GaN heteroepitaxial nanorod EL devices, n-ZnO nanorods were vertically grown on 3 μm thick p-GaN layers coated on Al_2O_3 (0001) using catalyst-free MOVPE. The p-GaN layers exhibited a p-type carrier concentration of 2×10^{17} cm^{-3} and a mobility of 10 $cm^2 V^{-1} s^{-1}$. For ZnO nanorod MOVPE growth, diethyl-zinc (DEZn) and oxygen were employed as reactant sources, as previously reported [13]. Details in the growth parameters of ZnO nanorods on GaN substrates are the same as those on sapphire substrates except for the DEZn flow prior to ZnO growth. That is, in the initial ZnO growth stage, only DEZn with a carrier gas flowed for 30 s prior to ZnO nanorod growth in order to prevent GaN surface oxidation.

The EL devices were fabricated by making good ohmic contacts on both p-GaN and n-ZnO. The ohmic contact on p-GaN was fabricated by evaporating Pt and Au bilayers. The typical Pt and Au layer thicknesses were 100 Å and 500 Å, respectively. After the metallization of p-GaN, the free space between the individual ZnO nanorods was filled with a thin photoresist by spin coating. This was followed by selective etching of the photoresist under an oxygen plasma in order to produce a nanorod array embedded in the photoresist with only the nanorod tips exposed (by 50–100 nm; Fig. 1c). For the metallization of the n-ZnO nanorods, 100 Å thick Ti and 500 Å thick Au layers were deposited on the nanorod tips through a shadow mask by electron-beam evaporation, resulting in a continuous contact layer on the ZnO nanorods (Fig. 1d). Good ohmic contacts on both n-ZnO and p-GaN were made by rapid thermal annealing at 300 and 500 °C for 1 min, respectively. The EL and *I–V* characteristics of the devices were measured by applying a DC voltage to the device using a source meter (Keithley 2400). The EL spectra were measured using a monochromator and a detection system equipped with a photomultiplier tube and a photon counter which had been used for photoluminescence spectroscopy [3]. All measurements were preformed at room temperature.

Received: July 21, 2003
Final version: September 30, 2003

[1] W. Y. Liang, A. D. Yoffe, *Phys. Rev. Lett.* **1968**, *20*, 59.
[2] P. Zu, Z. K. Tang, G. K. L. Wong, M. Kawasaki, A. Ohtomo, H. Koinuma, Y. Segawa, *Solid State Commun.* **1997**, *103*, 459.
[3] S. W. Jung, W. I. Park, H. D. Cheong, G.-C. Yi, H. M. Jang, S. Hong, T. Joo, *Appl. Phys. Lett.* **2002**, *80*, 1924.
[4] M. H. Huang, S. Mao, H. Feick, H. Yan, Y. Wu, H. Kind, E. Weber, R. Russo, P. Yang, *Science* **2001**, *292*, 1897.
[5] W. I. Park, Y. H. Jun, S. W. Jung, G.-C. Yi, *Appl. Phys. Lett.* **2003**, *82*, 964.
[6] W. I. Park, G.-C. Yi, M. Kim, S. J. Pennycook, *Adv. Mater.* **2003**, *15*, 526.
[7] R. D. Vispute, V. Talyansky, S. Choopun, R. P. Sharma, T. Venkatesan, M. He, X. Tang, J. B. Halpern, M. G. Spencer, Y. X. Li, L. G. Salamanca-Riba, A. A. Iliadis, K. A. Jones, *Appl. Phys. Lett.* **1998**, *73*, 348.
[8] S.-K. Hong, T. Hanada, H. Makino, Y. Chen, H.-J. Ko, T. Yao, A. Tanaka, H. Sasaki, S. Sato, *Appl. Phys. Lett.* **2001**, *78*, 3349.
[9] a) X. Duan, Y. Huang, Y. Cui, J. Wang, C. M. Lieber, *Nature* **2001**, *409*, 66. b) X. Duan, Y. Huang, R. Agarwal, C. M. Lieber, *Nature* **2003**, *421*, 241.
[10] M. W. Wang, J. O. McCaldin, J. F. Swenberg, T. C. McGill, R. J. Hausnstein, *Appl. Phys. Lett.* **1995**, *66*, 1974.
[11] G. D. J. Smit, S. Rogge, T. M. Klapwijk, *Appl. Phys. Lett.* **2002**, *81*, 3852.
[12] W. I. Park, G.-C. Yi, J.-W. Kim, S.-M. Park, *Appl. Phys. Lett.* **2003**, *82*, 4358.
[13] W. I. Park, D. H. Kim, S.-W. Jung, G.-C. Yi, *Appl. Phys. Lett.* **2002**, *80*, 4232.
[14] D. C. Reynolds, D. C. Look, B. Jogai, *J. Appl. Phys.* **2001**, *89*, 6189.
[15] M. A. Reshchikov, G.-C. Yi, B. W. Wessels, *Phys. Rev. B* **1999**, *59*, 13 176.
[16] M. Kim, W. I. Park, G.-C. Yi, unpublished.
[17] J. Neugebauer, C. G. Van de Walle, *Phys. Rev. Lett.* **1995**, *75*, 4452.
[18] S. Sze, *Physics of Semiconductor Devices*, 2nd ed., Wiley, New York **1981**, Ch. 2.
[19] T. Nakayama, M. Murayama, *J. Cryst. Growth* **2000**, *214*, 299.

Preparation of Arrays of Isolated Spherical Cavities by Self-Assembly of Polystyrene Spheres on Self-Assembled Pre-patterned Macroporous Films

By *Mamdouh E. Abdelsalam*, *Philip N. Bartlett*,* *Jeremy J. Baumberg*, and *Steve Coyle*

Self-assembly of colloidal spheres onto patterned (e.g., lithographically modified)[1] substrates is a promising approach to prepare complex three-dimensional (3D) geometries (e.g., assemble colloidal spheres into square pyramidal shapes)[2] that cannot be produced by self-assembly of colloidal spheres on flat substrates. Generally self-assembly alone is restricted to the formation of close-packed two-dimensional (2D) and 3D arrays of colloidal particles and does not lead to more complex lattice types and geometries. A certain degree of control over colloidal self-assembly has been achieved through external electric[3] or intense optical fields[4] and by manipulating the interaction potential.[5] Here, we demonstrate a simple scheme that combines two self-assembly steps and electrochemical deposition to produce patterns of ordered arrays of spheres with controlled spacing and eventually isolated metallic arrays of spherical cavities. First, the substrate was pre-patterned by electrochemical deposition through templates of polystyrene spheres assembled as a hexagonal-close-packed monolayer on an evaporated gold surface. This was followed by removal of the template by dissolution in tetrahydrofuran (THF). Then monodisperse polystyrene spheres were allowed to slowly assemble on the pre-patterned substrate in a purpose-built cell. Finally, electrochemical deposition through the top layer of spheres was achieved to produce the final 3D structure; the schematic illustration of this procedure is shown in Figure 1. Electrochemical deposition has a number of significant advantages. It produces a high density deposited material and no shrinkage of the material takes place when the template is removed.

[*] Prof. P. N. Bartlett, Dr. M. E. Abdelsalem
School of Chemistry, University of Southampton
Southampton, SO17 1BJ (UK)
E-mail: P.N.Bartlett@soton.ac.uk
Prof. J. J. Baumberg, S. Coyle
School of Physics and Astronomy
University of Southampton
Southampton, SO17 1BJ (UK)

  DOI: 10.1002/adma.200306052